

Title	Silicon photonics-based laser Doppler vibrometer array for carotid-femoral pulse wave velocity (PWV) measurement
Authors	Li, Yanlu;Marais, Louise;Khettab, Hakim;Quan, Zhiheng;Aasmul, Soren;Leinders, Rob;Schüler, Ralf;Morrissey, Padraic E.;Greenwald, Stephen;Segers, Patrick;Vanslebrouck, Michael;Bruno, Rosa M.;Boutouyrie, Pierre;O'Brien, Peter;de Melis, Mirko;Baets, Roel
Publication date	2020-06-22
Original Citation	Li, Y., Marais, L., Khettab, H., Quan, Z., Aasmul, S., Leinders, R., Schüler, R., Morrissey, P. E., Greenwald, S., Segers, P., Vanslebrouck, M., Bruno, R. M., Boutouyrie, P., O'Brien, P., de Melis, M. and Baets, R. (2020) 'Silicon photonics-based laser Doppler vibrometer array for carotid-femoral pulse wave velocity (PWV) measurement', Biomedical Optics Express, 11(7), pp. 3913-3926. doi: 10.1364/BOE.394921
Type of publication	Article (peer-reviewed)
Link to publisher's version	10.1364/BOE.394921
Rights	© 2021, Optical Society of America under the terms of the OSA Open Access Publishing Agreement.
Download date	2024-07-07 04:07:40
Item downloaded from	https://hdl.handle.net/10468/11081




UCC

University College Cork, Ireland
Coláiste na hOllscoile Corcaigh



Silicon photonics-based laser Doppler vibrometer array for carotid-femoral pulse wave velocity (PWV) measurement

YANLU LI,^{1,2,*} LOUISE MARAIS,³ HAKIM KHETTAB,³ ZHIHENG QUAN,⁴ SOREN AASMUL,⁵ ROB LEINDERS,⁵ RALF SCHÜLER,⁶ PADRAIC E. MORRISSEY,⁴ STEPHEN GREENWALD,⁷ PATRICK SEGERS,⁸ MICHAEL VANSLEMBROUCK,^{1,2} ROSA M. BRUNO,³ PIERRE BOUTOUYRIE,³ PETER O'BRIEN,⁴ MIRKO DE MELIS,⁵ AND ROEL BAETS^{1,2} 

¹Photonics Research Group, Ghent University-imec, Technologiepark-Zwijnaarde 126, 9052, Ghent, Belgium

²Center for Nano- and Biophotonics, Ghent University, Technologiepark-Zwijnaarde 126, 9052, Ghent, Belgium

³INSERM U970, Université de Paris, Assistance Publique Hôpitaux de Paris, Paris, France

⁴Photonic Packaging Group, Tyndall National Institute, Lee Maltings Complex Dyke Parade, T12R5CP, Cork, Ireland

⁵Medtronic Bakken Research Center, Endepolsdomein 5, 6229 GW, Maastricht, The Netherlands

⁶SIOS Messtechnik GmbH, Am Vogelherd 46, 98693, Ilmenau, Germany

⁷Blizard Institute, Barts and The London School of Medicine and Dentistry, Queen Mary University of London, E1 2AT, London, UK

⁸IBiTech-bioMMeda, Ghent University, De Pintelaan 185, 9000, Ghent, Belgium

*Yanlu.Li@UGent.be

Abstract: Pulse wave velocity (PWV) is a reference measure for aortic stiffness, itself an important biomarker of cardiovascular risk. To enable low-cost and easy-to-use PWV measurement devices that can be used in routine clinical practice, we have designed several handheld PWV sensors using miniaturized laser Doppler vibrometer (LDV) arrays in a silicon photonics platform. The LDV-based PWV sensor design and the signal processing protocol to obtain pulse transit time (PTT) and carotid-femoral PWV in a feasibility study in humans, are described in this paper. Compared with a commercial reference PWV measurement system, measuring arterial pressure waveforms by applanation tonometry, LDV-based displacement signals resulted in more complex signals. However, we have shown that it is possible to identify reliable fiducial points for PTT calculation using the maximum of the 2nd derivative algorithm in LDV-based signals, comparable to those obtained by the reference technique, applanation tonometry.

© 2020 Optical Society of America under the terms of the [OSA Open Access Publishing Agreement](#)

1. Introduction

Arteries are elastic structures that distend with each contraction of the heart in systole and elastically recoil in diastole, during which the stored elastic energy works on the blood. They thereby buffer the pulsatile action of the heart, damping the pressure pulsations within them and reducing the pulsatility of blood flow so that organs are continuously provided with blood (and oxygen and nutrients). As the aorta is the largest contributor to this buffering action, measurement of aortic stiffness has received much attention. Over the last decades, increasing evidence has accumulated demonstrating that increased aortic stiffness is an important risk factor for cardiovascular disease (CVD) [1]. Measurement of aortic stiffness at the primary care level would allow screening large populations for cardiovascular (CV) risk and thus enable more accurate CV

risk prediction to better target preventive therapy among those individuals considered to be at low or moderate risk, as defined by current guidelines. However, its widespread use is limited by its relative complexity. Portable, low-cost, point-of-care screening devices for reliable, fast and non- or minimally-invasive measurement of aortic stiffness are thus strongly needed.

Pulse wave velocity (PWV) is the speed at which a mechanical perturbation, induced by the ejection of the blood from the left heart chamber, propagates along the arteries. It is usually calculated as the ratio of the path length traveled by the perturbation and the pulse transit time (PTT), the time that is needed for the perturbation to travel the path length. According to the Moens Korteweg equation [2], the PWV value is proportional to the square root of the elastic modulus of the aorta. Therefore, a higher value of PWV indicates a greater arterial stiffness and thus a greater load on the heart and arteries and, consequently, a higher risk of cardiovascular (CV) events. Aortic stiffness can be measured in a number of ways, but the non-invasive measurement of the carotid-femoral pulse wave velocity (cf-PWV), a proxy for aortic pulse wave velocity (aPWV), is regarded as the current gold standard [3]. This has been demonstrated in many populations worldwide [4,5]. The cf-PWV is usually measured by the use of two sensors applied on two separate places on the body: one is on the skin above the carotid artery and the other is above the femoral artery near the groin. The sensors can be pressure sensors (piezo-electric sensors or applanation tonometers [6]), ultrasound devices [6] or photoplethysmographic sensors [7]. Several commercially available devices have been introduced, the most well-known being the Complior [6], using piezoelectric sensors, and SphygmoCor system, using applanation tonometers [8]. At present, however, none of the devices are deemed suitable for use in a primary care setting due to several issues. Firstly, Complior and SphygmoCor have pressure probes which need to be applied to the skin overlying the artery of interest in order to partially compress them and obtain pressure waves: since obtaining a good signal is highly dependent on the correct positioning of the probes, experienced operators are needed. Pressure waves of altered morphology also make identification of fiducial points difficult and induce uncontrollable biases. Secondly, these systems are usually expensive. In addition, they sometimes cause discomfort to subjects because the sensors may involve palpation and compression of the groin and the neck. Some cuff-based devices have tried to resolve some of these limitations [9], but, since they are applied to peripheral vessels (ankle and wrist), they do not yield direct measurement of aortic stiffness, the principal part of the arterial buffering function, and thus, their clinical has been questioned [10]. Others [11] are sometimes impractical because of the use of cuffs around the neck, an experience not well tolerated by most patients, or do not measure pulse transit times directly and do not reliably yield values that correspond to those derived by direct PWV methods [12]. As a result, although it has been recognized that aortic stiffening is an important and early “phenotype” of vascular ageing and that its measurement is useful for the assessment and stratification of total CV risk, still it is not routinely measured in primary care.

Laser Doppler vibrometry (LDV) is a vibration-sensing technique that conducts non-contact measurement of the displacement or velocity of a vibrating/moving target by means of a probing laser beam [13]. The LDV recovers the target movement information by analyzing the Doppler phase/frequency shift of the reflection signal, which is proportional to the instantaneous displacement/velocity of the target. The displacement resolution of LDV can achieve the picometer or femtometer range [14]. Such a high sensitivity is obtained mainly thanks to the high frequency stability of the laser signal. Since skin motion due to underlying arterial pulsations are in the sub-millimeter range (i.e. they are easily sensed by finger palpation over superficial arteries such as the carotid and femoral), they are therefore measurable using LDV, as previously demonstrated [15,16]. LDV has previously been used for the non-contact detection of the carotid pulse, both as a means of measuring blood pressure [17] and, more generally, for deriving physiological information from its shape and timing [18]. However, medical applications of industrial LDV systems for PWV measurement have been limited by the fact that they are built

on discrete optics and thus are bulky and expensive. To enable a relatively low-cost and compact LDV system, we have designed and developed several different LDVs [19] in a silicon-based photonic integrated circuit (PIC) platform. Thanks to the use of CMOS-compatible techniques, this platform has the potential to be low-cost with high-to-moderate production volume [20]. The compact size of the PIC-based device enables an easy realization of multi-beam LDV systems, which can simplify the process of PWV measurements. The LDV sensor for the PWV measurement proposed in this paper has two compact sensor heads, each with 6 sensing beams arranged in a line which is orientated at right angles to the long axis of the underlying artery. Thus, one or more of the sensing beams will coincide with the arterial path and the maximum pulse may be obtained without aiming precisely over the artery. Moreover, the LDV array allows the acquisition of carotid and femoral pulses simultaneously, thus it does not require ECG signal recording, which is sometimes used in other systems for the resynchronization of sequentially acquired carotid and femoral pulse waves. A detailed description of the LDV sensor will be given in the next section.

The objectives of the present paper are to describe the configuration and design of the complete sensing system. Then we will describe the first clinical applications and steps in the signal management necessary before performing a feasibility study in human subjects.

2. LDV-array design and system calibration

In the proposed device, each sensor head can simultaneously measure vibrations at six locations in a line with a 5 mm spacing (see Fig. 1(a)). This spacing value is chosen to ensure the locations with strong pulse movements are not missed by at least one of the measurement beams. As a result, the sensor allows for accurate measurements on at least one pair of beams without having to target precisely the artery. The overall system includes three major parts: two optical sensor heads, an electrical rack and a personal computer (PC) (Fig. 1(b)). The sensor heads are the parts that generate the sensing optical beams, receive the corresponding reflections, and convert the received optical signals to electrical signals. Each sensor head consists of one PIC with six sensing LDVs, one integrated laser source, one optical system, one aluminum (Al) passive cooler and a printed-circuit board (PCB) for laser drive and signal conditioning. The electrical rack realizes the analog-to-digital conversion (ADC) for the electrical signals sent from the sensor heads. The unprocessed signals are then sent to the PC, where they are saved for signal demodulation and further analysis.

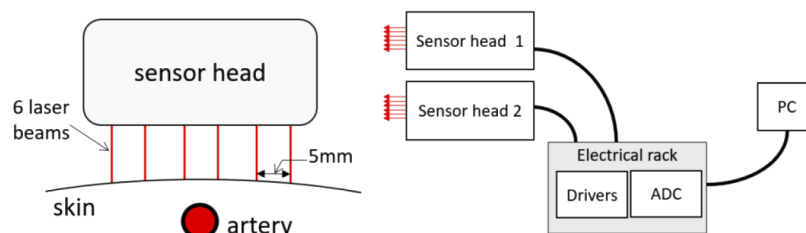


Fig. 1. (a) The configuration of the six-beam sensor head. (b) The three major parts of the PWV measurement system.

The two hand pieces can measure vibrations simultaneously and allow for flexible use of the device for different applications (see Fig. 2). When the two locations are close to each other, the two hand pieces are aligned and held together with magnets. By placing a hand-piece spacer with a certain thickness between the two hand pieces, the distance of the two sensors can be adjusted. The minimal distance is 25 mm when no hand-piece spacer is used.

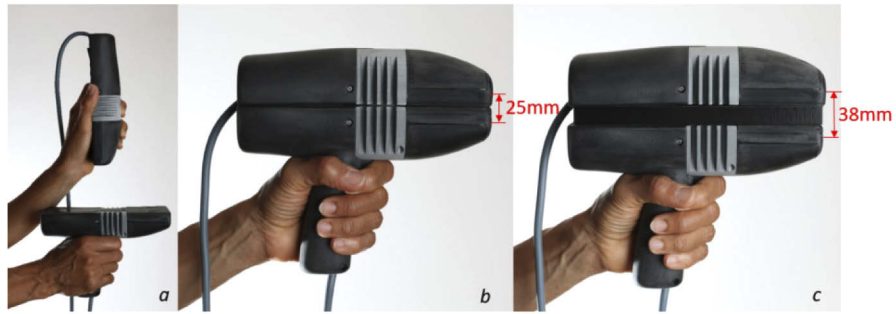


Fig. 2. Different ways of using the two sensor heads. *a.* Detached. *b.* Attached without spacer. *c.* Attached with a spacer (13 mm). Note the sensor heads in the figures are non-functional 1:1 models with different colors from the working devices.

All sensing beams operate in the invisible infrared wavelength range (1550 nm). This is determined by the PIC platform (silicon-on-insulator) which has the best performance in this wavelength range. However, the operators need to know the sensing locations during the measurement. To improve the usability, we designed an aiming beam system in these devices with two red (650 nm) laser diodes at either side of the sensor head, each projecting a cross pattern onto the skin (see Fig. 3(a)). The angles and directions of these red laser diodes are adjusted and fixed in the packaging step such that the two crosses overlap at the focal plane of the lens system, while the focus points of the six infrared sensing beams lie on the horizontal line of the overlapped aiming beams. With the help of these aiming beams, one can ensure that the target is placed at the right location and with the right working distance. In addition to the aiming beams, we also prepared physical sensing spacers that can be attached to the front of each sensor head. The task of the spacers is to maintain the correct distance between the sensor head and the measurement target, and to avoid unwanted relative movements between the operator and the subject under test. One example is shown in Fig. 3(b). The front of the spacer has a curved surface, so that the pressure wave is not blocked by the spacer.

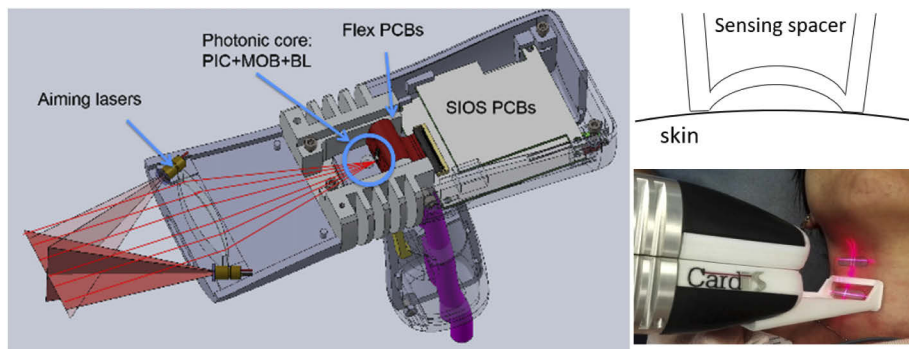


Fig. 3. (a) The inside of the photonic head. PIC stands for photonic integrated circuit, MOB stands for micro-optical bench and BL stands for ball lens. (b) the use of the sensing spacers.

The part that handles the optical signals is the PIC present in each sensor head. The performance of the six-beam LDV PIC has been reported in [16], so here we only summarize the basic working principle of the LDV PIC. Each LDV circuit is based on an on-chip optical Mach-Zehnder interferometer (MZI). In each chip, the six MZIs share the same input light via one 20:80 splitter and two 1-by-6 splitters (Fig. 4). The 20:80 splitter ensures that more light power goes to the

sensing beams so that the signal-to-noise ratios of the LDV signals are optimized. Each MZI circuit sends one sensing beam out of the silicon-on-insulator chip via a grating-coupler-based transmitting antenna (TA). The six TAs are placed in a line with a spacing of $300\ \mu\text{m}$ to ensure the spacing is large enough to avoid significant cross talk between the TAs. Meanwhile, the chip (with a width of $2.5\ \text{mm}$) is still large enough to place all the six LDVs with this TA spacing. A grating coupler-based receiving antenna (RA) is placed next to each TA to collect any light sent out from the corresponding TA after reflection by the target. The reflected light and a reference signal that is directly retrieved from the source are combined in a 90° -degree optical hybrid [21] on the chip. Four on-chip germanium photo-diodes are connected to the four outputs of the 90° -degree optical hybrid. With the four photo-current signals, one can retrieve the phase change in the measurement signal with an IQ demodulation technique [19]. The demodulated signal is the displacement of the target. The corresponding velocity and acceleration signals can be derived using the first and second derivative of the displacement signals.

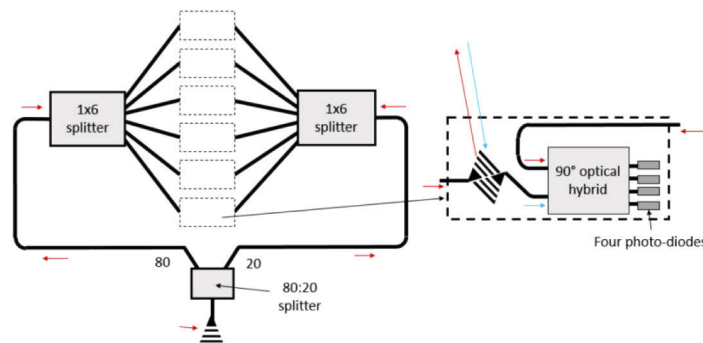


Fig. 4. Schematic showing the PIC design with six LDVs.

Unlike the previously reported design [16] in which the laser signals are coupled to the PIC via a fiber, in this demonstrator each sensor head has its integrated laser source on the LDV PIC in a form of a micro-optical bench (MOB) [22]. The MOB consists of a ceramic bench, a laser source, an optical isolator, two micro ball lenses and a prism mirror to change the orientation of the laser beam to a downward direction so as to couple the light into the PIC. The use of a MOB is to ensure a compact system with a stable laser source and to avoid any fiber connections which can move. The $1550\ \text{nm}$ laser source is a distributed-feedback (DFB) laser diode with a linewidth of $800\ \text{kHz}$. A schematic of the MOB design and a side-view optical microscope image are shown in Fig. 5(a). The optical isolator is used to avoid back-reflection to the laser source, as this may affect the stability of the laser source and induce a complicated self-mixing phenomenon therein [23]. The optical isolation of the optical bench is $> 20\ \text{dB}$.

The PIC with the MOB is placed on an Al submount, where a flexible PCB is also glued next to the PIC (Fig. 5(b)). The PIC's electrical pads are wire-bonded to bond pads of the flexible PCB. The flexible PCB is used to plug into the main PCB populated with the transimpedance amplifiers (TIAs). The PIC and the flexible PCB are connected using wire-bonding. The laser source as well as the MZI requires a stable wavelength during operation, which is normally obtained by temperature stabilization. However, it was found that the circuitry required to control a thermoelectric cooling (TEC) system produced excessive heat, which raised the overall temperature of the assembly out of specification. Therefore, the TEC was not used in this device. Instead the aluminum (Al) submount as well as the PIC are used as the heat conductor between the integrated laser MOB and the heat sink, i.e. passive Al cooler. Experiments showed that the large Al heat sink was sufficient to dissipate the heat generated from the MOB laser without the use of a TEC and thus to stabilize the temperature.

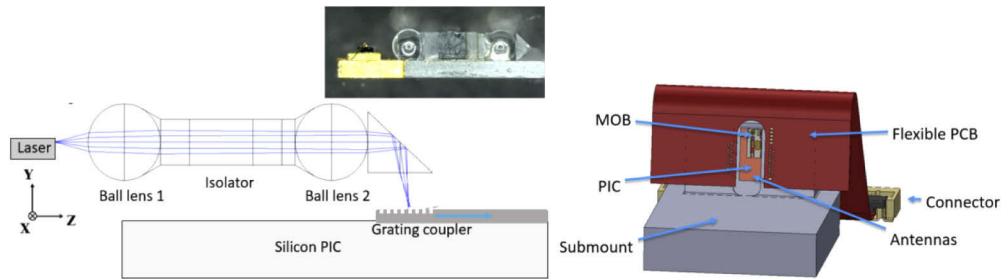


Fig. 5. (a) Schematic of the MOB design and a side-view microscope image of the MOB. (b) The mounting of the PIC with PCB.

A confocal optical system [16] is placed in each sensor head (see Fig. 3(a)). A schematic show of the system is shown in Fig. 6. The lens close to the PIC is a ball lens with a diameter of 1.4 mm, while the other lens is a double-convex lens with a focal length of 71 mm. The two lenses are placed in the optical axis of the system such that their focal points overlap. When the source is placed on the focal plane of the ball lens, the light beams will be focused on the focal plane of the big lens. The optical system ensures all six output beams are focused to the target on six evenly spaced spots from the same direction, while the reflection strength coupled back to the single mode waveguide is also good enough (verified by Zemax simulation). This lens system is simple to assemble and the alignment procedure is easy. However, the optical system is still a bit bulky. To enhance the signal strength, a micro-beads based retroreflective sticker is placed on the target.

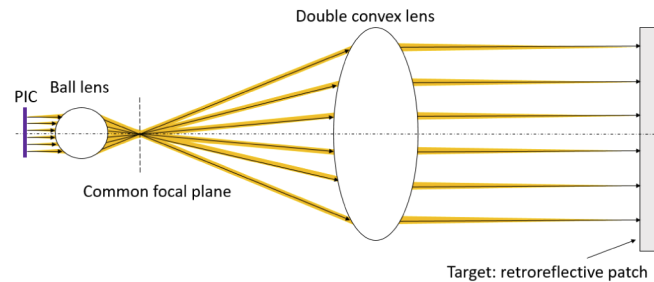


Fig. 6. Schematic show of the optical system. The sizes of the lenses and PIC are exaggerated in the figure to clearly show the configuration of the lens system.

The high impedance outputs of the PDs are decoupled with a set of TIAs close to the PIC. The four PDs in the same optical hybrid are connected in common anode mode. The photo-current signals are passed through two amplification stages. In the first stage, four separate TIAs amplify all four photocurrents. In the second stage, two sets of differential amplifiers combine two signals each in antiphase. With these TIAs, the voltage amplitudes can reach hundreds of millivolts to volts before being sent to the data acquisition (DAQ) system in the electrical rack and then stored in the PC. The DAQ system obtained the signal with a sample frequency of 100 kS/s for each channel. This sample frequency is chosen to obtain a maximal vibration velocity of around 40 mm/s, which is higher than the maximal measured pulse velocity obtained in previous test measurements. The signals are saved in the PC and are then demodulated for post-processing. A real-time view of the demodulated signal can also be displayed on the PC-screen during the measurement.

The optical power levels of the beams toward the target are measured at the target plane with a power meter to be between $20 \mu\text{W}$ and $40 \mu\text{W}$, which is far below the laser safety power limit for this wavelength (10 mW). The positions of the sensing spots are calibrated with a black shading plate that has six holes corresponding to the spacing of the sensing beams (see Fig. 7(a)). The diameter of the holes is set at 3 mm . Results show that all the beams are passed through the holes simultaneously, thus establishing that the sensing beams are sent to the desired locations.

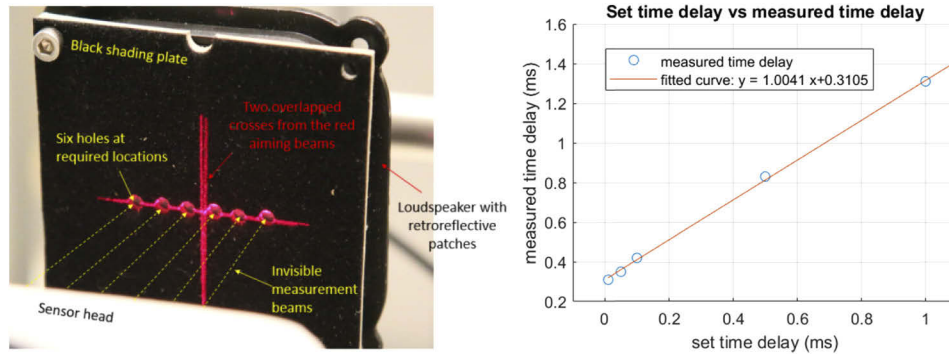


Fig. 7. (a) The target used to test the positions of the output beams. (b) the measured time delay vs set time delay for the time delay measurement (note the 5 ms sample is omitted from the plot to allow the fit of the shorter delay times to be more clearly seen).

To ensure a PWV measurement can be made with a good resolution, we also measure the time delay by directing the beams from the two sensor heads on to two loudspeakers. The loudspeakers have a flat moving membrane which moves in a plane normal to the beam direction, which has been measured and specified with a SIOS Nanoanalyzer vibration analysis tool [24]. We generate two acoustic pulses with a dedicated time delay in the two loudspeakers separately. The time delay is changed from $1 \mu\text{s}$ to 5 ms in a series of measurements. The relationship between the measured time delay and the set time delay is shown in Fig. 7(b). The results show a strong linear relation between the measured time delay and the set time delay (with the coefficient of determination being equal to 1). It has been verified that the offset in the y direction ($310 \mu\text{s}$) is caused by the inherent difference in response delay between the two loudspeakers. Therefore, the time delay measurement is accurate enough for the PWV measurement, which requires a resolution of $25 \mu\text{s}$.

3. Signal analysis

3.1. Study protocol

Carotid-femoral PWV is calculated by dividing traveled distance by PTT, making it crucial to correctly measure PTT. The aims of the study were to set up the best methodology to measure the PTT with multibeam LDVs. Data for this analysis were obtained during the clinical feasibility study, aimed at validating LDV carotid-femoral PWV against the reference technique, applanation tonometry [25], according to the protocol set up in current guidelines [26]. The main results of the clinical feasibility study (NCT03446430), enrolling 100 patients of both sexes (50/50) having controlled or uncontrolled hypertension, will be published in a separate paper. The signal analysis protocol, summarized in the present paper, was developed from the recordings of 20 patients randomly selected from this population. All patients agreed to participate and signed an informed consent document, which was reviewed and accepted by a French National Ethics Committee. All signal processing and data management was done blind to the patients' characteristics and blind to the PWV values obtained by the reference methods. During the whole process and after,

patients' data were only identified through a code number, the contingency list was kept by the principal investigator in a safe.

For LDV assessment, patients had the retroreflective stickers applied to the skin over the right common carotid (anterior to the sternocleidomastoid muscle) and femoral artery (close to the inguinal ligament), orthogonal to the supposed main axis of the artery. The LDV cf-PWV were measured with one six-beam LDV sensor head targeting the carotid (LDV1) and the other the femoral artery (LDV2, Fig. 8(a)). Four acquisitions of 20 seconds were performed. One synchronous ECG lead was recorded too. Surface distance between the two measurement points was measured by a tape measure in a straight line. Traveled distance for PWV calculation was obtained as the direct distance between carotid and femoral site, multiplied by 0.8, according to current guidelines [25].

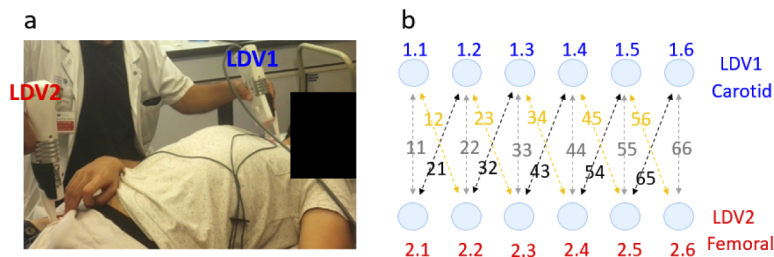


Fig. 8. (a) A picture of the measurement setting for carotid-femoral PWV. The two sensor heads of the LDV device are detached and positioned simultaneously on the carotid site (LDV1) and on the femoral site (LDV2). An ECG signal is simultaneously recorded. (b) Schematic representation of the 16 beam combinations for PTT calculation, arising by analysis of the 6 sensing beams from LDV1 sensor head, on the carotid site (beams 1.1 to 1.6) and the 6 sensing beams from LDV2 sensor head, on the femoral site (beams 2.1 to 2.6).

3.2. Channel selection

Since each LDV sensor head has a row of six laser beams (LDV1: from beam 1.1 to beam 1.6; LDV2: from beam 2.1 to beam 2.6, see Fig. 8(b)), 36 PTT calculations of pulse transit time are possible, between the beams of the two laser beam rows. However, in order to reduce processing time, for each beam, the PTT was calculated considering the facing one (i.e. PTT between beam 1.2 on LDV1 and 2.2 on LDV2) and the diagonal ones shifted by only one position (i.e. between beam 1.2 on LDV1 and beam 2.1 and 2.3 on LDV2), leading to 16 beam combinations (Fig. 8(b)). Two combinations (between beam 1.6 on LDV1 and beam 2.5 and 2.6 on LDV2) gave poor results, with beat-to-beat PWV standard deviation greater than 3 m/s, and thus were excluded. The major reason for the poor results is the low signal quality of the signal for channel 1.6, which measured at a location that was not covered by the reflective patch. Then, the median PWV from the 14 remaining combinations was derived and considered as the final PWV value. Finally, we considered the median PWV from the 4 acquisitions per patient as the final result.

3.3. Algorithms for PTT calculation (ECG-dependent)

In-house algorithms were developed using MATLAB to post-process the LDV signals and calculate PTT between the two laser beam rows. Classical processing methods to derive the PTT from arterial pulse waves consist of the identification of a fiducial point on each signal, usually the foot of the pressure wave, using either intersecting tangents, or the maximum of the 2nd derivative, or the 10% upstroke [27]. These methods have been shown to be accurate both on invasive and non-invasive arterial pressure waveforms [28] and some of them have been applied to commercial devices, such as the SphygmoCor system (AtCor Medical), used as comparator

in the present study. Conversely, it is crucial to determine which methods may be suitable to analyze LDV displacement signals, which may present relevant differences compared to pressure waveform signals.

First, we optimized raw signal filtering and differentiation in order to get clear acceleration signals. The LDV displacement signals from the 12 beams and the ECG signal were retrieved with MATLAB from the raw acquisition files and down sampled to a sample rate of 10 kHz using in-house codes. The displacement signals were differentiated twice to get acceleration signals and filtered (low-pass filter frequency 30 Hz) to remove the noise introduced by differentiation.

In this phase, the ECG signal was used to identify the heartbeats and the correct time-points (foot of the wave, dicrotic notch): the Matlab function 'findpeaks.m' was used to identify the R-peaks. For each heartbeat individually, we then searched for peaks in the carotid and femoral acceleration signals within an acceptable time interval (R-peak time + 2 to 17% of mean heartbeat duration for carotid, R-peak time + 6 to 26% of mean heartbeat duration for femoral). The highest carotid peak found was selected as fiducial point. Then, femoral peaks yielding pulse wave velocities below 3 m/s or above 20 m/s were discarded and the highest remaining peak was selected. Transit times were calculated for all the heartbeats and outlier values (more than three scaled median absolute deviations away from the median) were removed. Finally, the mean and standard deviation (SD) of PWV were calculated.

For the tonometric signals, access to raw Sphygmocor data was not possible. However, the proprietary software allows exportation of pressure and ECG waveform data (already having undergone filter processing) at a sampling rate of 128 Hz. These signals were elaborated with Matlab as well, in order to derive acceleration signals and identify fiducial points with the same methodology applied to the LDV signals.

In Fig. 9 and Fig. 10, LDV and tonometry signals in three index subjects, a young, a middle-aged and an elderly individual, are shown. When looking at the shape of the LDV displacement signals, it is evident that it is very similar to the pressure waveform obtained by tonometry, for some patients but not for others; in particular, the foot of the wave is not always clearly visible. Indeed, it is conceivable that the displacement signal obtained by the LDV is more complex than the arterial pressure waveform, because it may incorporate vibrations coming from the muscular and subcutaneous tissues interposed between the artery and the skin. Also, measurements were taken with free breathing of the test subjects, leading to superimposed motions. Thus, it was not possible to apply the intersecting tangents or 10% upstroke algorithm to the vast majority of the recorded signals.

However, when we compared the acceleration signals (2nd derivative of the displacement signal from the LDV outputs), they exhibited more consistently the peak corresponding to the foot of the wave, even when the displacement signals did not reflect the tonometric waveforms (Fig. 9 and Fig. 10). Strikingly, in the acceleration signal from the carotid artery it is possible to constantly recognize a second peak, corresponding to the dicrotic notch (closure of the aortic valve, physiologically appearing within a time window of 250 to 450 ms after the first peak).

We therefore conclude that the maximum of the 2nd derivative is the most suitable algorithm for identification of fiducial points at each measurement site and thus for PTT and PWV assessment. The effectiveness of the 2nd derivative approach is in line with results obtained with other techniques, such as finger-toe PWV, using signals from photodiode sensors, rather than tonometric pressure waveforms, to calculate PWV [27].

3.4. Algorithms for PTT calculation (ECG-independent)

In order to move towards a completely contactless device, another algorithm was developed in order to identify heartbeats and the maximum of 2nd derivative without using ECG, based on cross correlation methods. The MATLAB algorithm makes it possible to automatically delimit

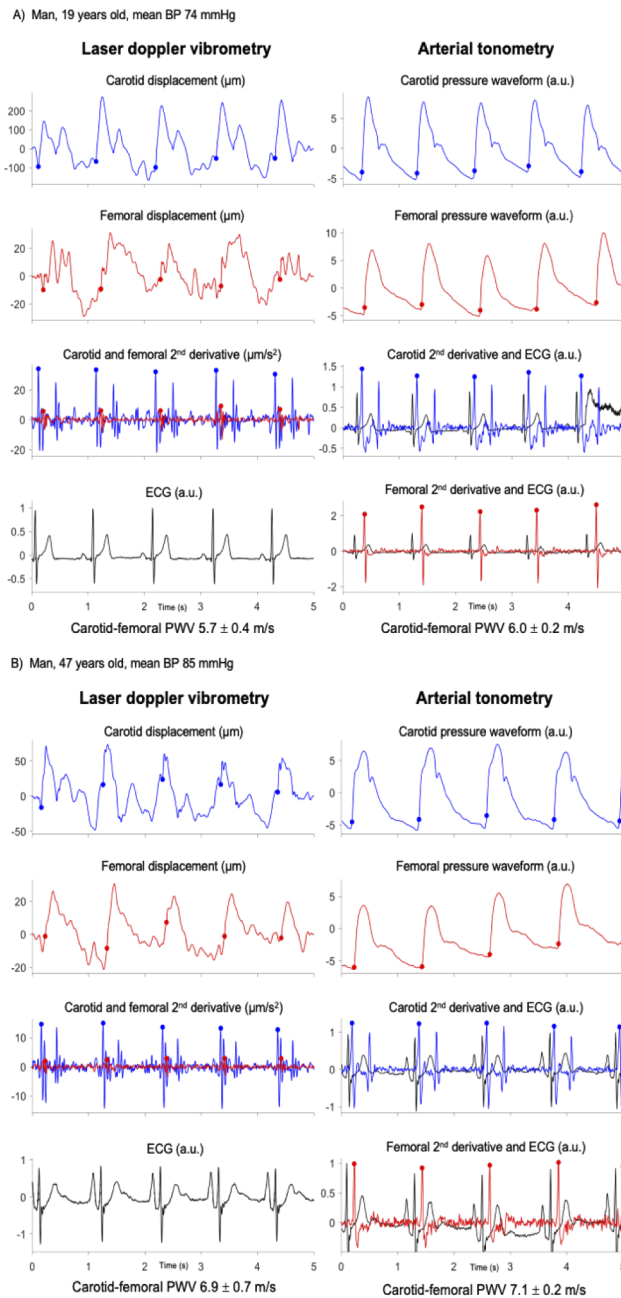


Fig. 9. Example of the displacement LDV signals (left) and tonometric arterial pressure waveforms (right) obtained from carotid and femoral measurements by LDV (one beam shown per location) in a young (a), a middle aged (b) individual. The corresponding acceleration signals exhibit peaks in systole, after the ECG R-peak, which allows identification of the wave-foot in both LDV and tonometric signals. A time delay between the acceleration peaks of the carotid (blue) and femoral (red) is clearly visible.

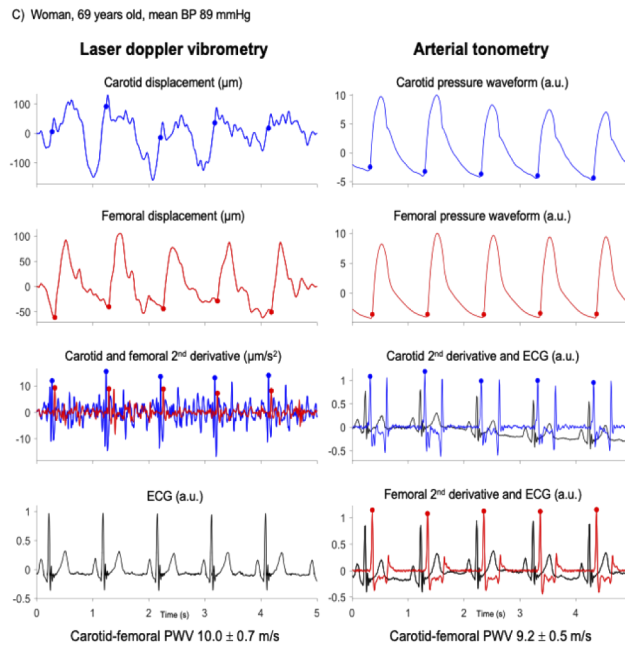


Fig. 10. Example of the displacement LDV signals (left) and tonometric arterial pressure waveforms (right) obtained from carotid and femoral measurements by LDV (one beam shown per location) in an old individual. A time delay between the acceleration peaks of the carotid (blue) and femoral (red) is clearly visible.

the heartbeats based on the identification of the carotid acceleration peaks (foot of the wave and diastolic notch), which have previously been shown to be consistently visible.

First, the mean period P of the carotid acceleration signal was estimated by autocorrelation. P is the time delay yielding the maximum of the correlation coefficient within a range of physiologically acceptable delay values (corresponding to heart rates between 30 and 100 bpm). The acceleration signal was then divided into successive segments of duration P which should correspond to successive heartbeats. For each segment, the time delays with respect to all other segments were estimated via cross correlation. Each segment was redefined by shifting its starting point by its median delay with respect to all other segments. This step allowed the synchronization of the segments and allows for the slight variations in heart rate around its mean value. The new durations (or periods) of the segments were calculated and outliers (segments with a duration 40% higher or lower than the median value) were identified and corrected: segments that were too long were split into two, while those that were too short were removed and incorporated into the preceding segment. Synchronization via cross correlation was then performed again until there were no outlier segments. After all the segments were delimited and synchronized, each segment signal was normalized to a value of 1 and all were averaged to calculate a mean heartbeat acceleration signal. Finally, the 'findpeaks.m' function was used to identify the two main peaks (foot of the wave and diastolic notch) separated by an interval between 250 and 450 ms. Once the carotid acceleration peaks corresponding to the foot of the wave were identified, we used the method described in the previous section (3.3) to search for femoral acceleration peaks in a time interval yielding acceptable PWV values (between 3 and 20 m/s) and calculated mean PWV.

The accuracy of the ECG-independent algorithm for PTT calculation was tested against the ECG-dependent algorithm described in Section 3.3. The correlation (Pearson $r = 0.960$, $p < 0.001$, Fig. 11(a)) between the two PTT values and the agreement between the two techniques

by Bland-Altman plot (Fig. 11(b)) were excellent. Bias between the two techniques (mean value 70.6 ± 14.5 ms for the ECG-independent algorithm vs 69.4 ± 14.5 ms for the ECG-dependent algorithm) was not significant (1.2 ms, 95% CL [-0.82; 3.18]). Similar results were obtained when PWV was calculated from the ECG-dependent or ECG-independent PTT: a non-significant bias of 0.12 m/s (95% CL 0.33; 0.08) was found, a difference without any relevance from the clinical point of view.

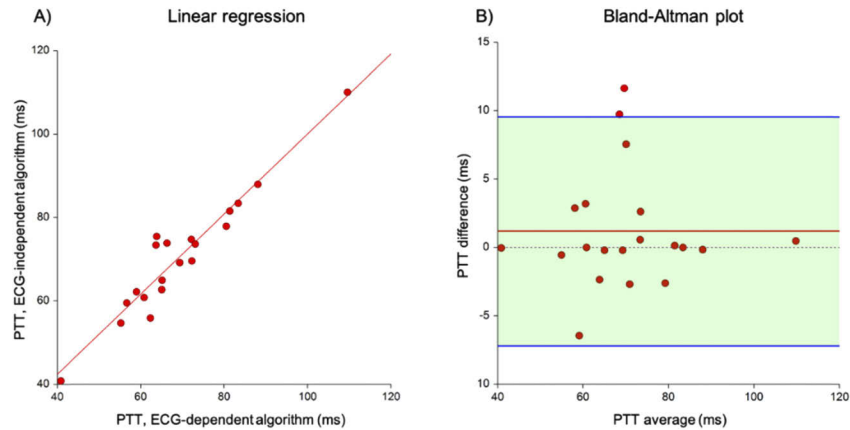


Fig. 11. Agreement between PTT calculated by means of ECG-dependent and ECG-independent algorithms. a) linear regression, equation PTT (ECG-independent algorithm) = $3.95 \pm 0.96 \times PTT$ (ECG-dependent algorithm). b) Bland Altman Plot. The red line represents the mean difference between PTT calculated by the ECG-independent and the ECG-dependent algorithm, whereas the blue lines represent its 95% confidence limits.

4. Conclusions and perspectives

We have developed a working prototype of a 2×6 beam laser Doppler vibrometer for the assessment of arterial stiffness in humans and established a signal analysis protocol for carotid-femoral PWV assessment, based on the 2nd derivative algorithm for foot detection, which is ECG-independent and thus allows a completely contactless assessment.

The potential advantages of the LDV-based PWV sensor include an easier alignment procedure, shorter measurement time, a simpler method to learn and less impact on the patient, in comparison to arterial tonometry, the reference technique. Thus, LDV-based PWV measurement is potentially applicable to large CVD screening campaigns and can be used by any health professional, including nurses and general practitioners. However, more data are needed in order to demonstrate reproducibility and agreement with the reference techniques. Furthermore, several design aspects of the LDV-based sensor should be improved to further enhance the usability, whereby the use of the reflective stickers should be avoided, for example by improving the optical power of the sensing beams.

An interesting design feature of the device is the possibility to attach the two sensor heads, which allows measurement of local PWV over a short arterial segment, such as the carotid artery. The distance between the two measurement sites can be set as small as 25 mm with the current sensor. This distance is not too short to make the PTT too small to detect, while it is also not too long to be suitable for most adults' neck length. In principle, this method is more appealing than the cf-PWV measurement since the common carotid artery has no side branches, is known to be a large elastic artery (while the aorta evolves from an elastic-type artery in the thorax to a more muscular artery in the abdomen) and follows a reasonably straight path. However, more

advanced signal processing may be required to analyse local carotid waveforms as they are likely to be contaminated by early wave reflections as found previously using ultrasound [29].

Funding

European Union's Horizon 2020 Framework Programme CARDIS project (644798).

Disclosures

The authors declare no conflicts of interest.

References

1. T. van Sloten, S. Sedaghat, S. Laurent, G. London, B. Pannier, M. Ikram, M. Kavousi, F. Mattace-Raso, O. Franco, P. Boutouyrie, and C. Stehouwer, "Carotid stiffness is associated with incident stroke: a systematic review and individual participant data meta-analysis," *J. Am. Coll. Cardiol.* **66**(19), 2116–2125 (2015).
2. W. Nichols and M. O'Rourke, *McDonald's Blood Flow in Arteries: Theoretical, Experimental, and Clinical Principles*, 4th ed (Edward Arnold, 1998).
3. The Reference Values for Arterial Stiffness' Collaboration, "Determinants of pulse wave velocity in healthy people and in the presence of cardiovascular risk factors: 'establishing normal and reference values'," *Eur. Heart J.* **31**(19), 2338–2350 (2010).
4. Y. Ben-Shlomo, M. Spears, C. Boustred, M. May, S. Anderson, E. Benjamin, P. Boutouyrie, J. Cameron, C. Chen, J. Cruickshank, S. Hwang, E. Lakatta, S. Laurent, J. Maldonado, G. Mitchell, S. Najjar, A. Newman, M. Ohishi, B. Pannier, T. Pereira, R. Vasan, T. Shokawa, K. Sutton-Tyrell, F. Verbeke, K. Wang, D. Webb, T. Willum Hansen, S. Zoungas, C. McEniery, J. Cockcroft, and I. Wilkinson, "Aortic pulse wave velocity improves cardiovascular event prediction: an individual participant meta-analysis of prospective observational data from 17,635 subjects," *J. Am. Coll. Cardiol.* **63**(7), 636–646 (2014).
5. C. Vlachopoulos, K. Aznaouridis, and C. Stefanadis, "Prediction of cardiovascular events and all-cause mortality with arterial stiffness: a systematic review and meta-analysis," *J. Am. Coll. Cardiol.* **55**(13), 1318–1327 (2010).
6. J. Calabria, P. Torquet, M. Garcia, I. Garcia, N. Martin, B. Guasch, D. Faur, and M. Vallés, "Doppler ultrasound in the measurement of pulse wave velocity: agreement with the Complior method," *Cardiovasc Ultrasound* **9**(1), 13 (2011).
7. S. Loukogeorgakis, R. Dawson, N. Phillips, C. Martyn, and S. Greenwald, "Validation of a device to measure arterial pulse wave velocity by a photoplethysmographic method," *Physiol. Meas.* **23**(3), 581–596 (2002).
8. M. Butlin and A. Qasem, "Large Artery Stiffness Assessment Using SphygmoCor Technology," *Pulse* **4**(4), 180–192 (2016).
9. V. Fabian, L. Matera, K. Bayerova, J. Havlik, V. Kremen, J. Pudil, P. Sajgalik, and D. Zemanek, "Noninvasive Assessment of Aortic Pulse Wave Velocity by the Brachial Occlusion-Cuff Technique: Comparative Study," *Sensors* **19**(16), 3467 (2019).
10. Y. Lu, M. Zhu, B. Bai, C. Chi, S. Yu, J. Teliewubai, H. Xu, K. Wang, J. Xiong, Y. Zhou, H. Ji, X. Fan, X. Yu, J. Li, J. Blacher, Y. Zhang, and Y. Xu, "Comparison of Carotid-Femoral and Brachial-Ankle Pulse-Wave Velocity in Association With Target Organ Damage in the Community-Dwelling Elderly Chinese: The Northern Shanghai Study," *J. Am. Heart Assoc.* **6**(2), e004168 (2017).
11. Y. Shahin, H. Barakat, R. Barnes, and I. Chetter, "The Vicorder device compared with SphygmoCor in the assessment of carotid-femoral pulse wave velocity in patients with peripheral arterial disease," *Hypertens. Res.* **36**(3), 208–212 (2013).
12. M. Ring, M. Eriksson, J. Zierath, and K. Caidahl, "Arterial stiffness estimation in healthy subjects: a validation of oscillometric (Arteriograph) and tonometric (SphygmoCor) techniques," *Hypertens. Res.* **37**(11), 999–1007 (2014).
13. S. Rothberg, M. Allen, P. Castellini, D. Di Maio, J. Dircks, D. Ewins, B. Halkon, P. Muyschondt, N. Paone, T. Ryan, H. Steger, E. Tomasini, S. Vanlanduit, and J. Vignola, "An international review of laser Doppler vibrometry: Making light work of vibration measurement," *Opt. Lasers Eng.* **99**, 11–22 (2017).
14. C. Rembe and R. Kowarsch, "High-Resolution Laser-Vibrometer Microscopy," *AMA Conferences 2017, Nuremberg Germany*, B5.3, (2017).
15. M. De Melis, U. Morbiducci, L. Scalise, E. Tomasini, D. Belbeke, R. Baets, L. Van Bortel, and P. Segers, "A noncontact approach for the evaluation of large artery stiffness: a preliminary study," *Am. J. Hypertens.* **21**(12), 1280–1283 (2008).
16. Y. Li, J. Zhu, M. Duperron, P. O'Brien, R. Schuler, S. Aasmul, M. De Melis, M. Kersemans, and R. Baets, "Six-beam homodyne laser Doppler vibrometry based on silicon photonics technology," *Opt. Express* **26**(3), 3638–3645 (2018).
17. L. Scalise, G. Cosoli, L. Casacanditella, S. Casaccia, and J. Rohrbaugh, "The measurement of blood pressure without contact: An LDV-based technique," *2017 IEEE International Symposium on Medical Measurements and Applications (MeMeA)*, Rochester, MN, 245–250 (2017).
18. S. Casaccia, E. Sirevaag, E. Richter, J. O'Sullivan, L. Scalise, and J. Rohrbaugh, "Features of the non-contact carotid pressure waveform: Cardiac and vascular dynamics during rebreathing," *Rev. Sci. Instrum.* **87**(10), 102501 (2016).

19. Y. Li and R. Baets, "Homodyne laser Doppler vibrometer on silicon-on-insulator with integrated 90 degree optical hybrids," *Opt. Express* **21**(11), 13342–13350 (2013).
20. W. Bogaerts, R. Baets, P. Dumon, V. Wiaux, S. Beckx, D. Taillaert, B. Luyssaert, J. Van Campenhout, P. Bienstman, and D. Van Thourhout, "Nanophotonic waveguides in silicon-on-insulator fabricated with CMOS technology," *J. Lightwave Technol.* **23**(1), 401–412 (2005).
21. R. Halir, G. Roelkens, A. Ortega-Monux, and J. Wanguemert-Perez, "High performance 90° hybrid based on a silicon-on-insulator multimode interference coupler," *Opt. Lett.* **36**(2), 178 (2011).
22. M. Duperron, L. Carroll, M. Rensing, S. Collins, Y. Zhao, Y. Li, R. Baets, and P. O'Brien, "Hybrid integration of laser source on silicon photonic integrated circuit for low-cost interferometry medical device," *Proc. SPIE* **10109**, 1010915 (2017).
23. G. Giuliani, M. Norgia, S. Donati, and T. Bosch, "Laser diode self-mixing technique for sensing applications," *J. Opt. A: Pure Appl. Opt.* **4**(6), S283–S294 (2002).
24. <https://sios-de.com/products/laser-vibrometer/nano-vibration-analyzer/>
25. L. Van Bortel, S. Laurent, P. Boutouyrie, P. Chowienczyk, J. Cruickshank, T. De Backer, J. Filipovsky, S. Huybrechts, F. Mattace-Raso, A. Protogerou, G. Schillaci, P. Segers, S. Vermeersch, T. Weber, and A. Society, "European Society of Hypertension Working Group on Vascular Structure and Function, and European Network for Noninvasive Investigation of Large Arteries: Expert consensus document on the measurement of aortic stiffness in daily practice using carotid-femoral pulse wave velocity," *J. Hypertens.* **30**(3), 445–448 (2012).
26. I. Wilkinson, C. McEniery, G. Schillaci, Pierre Boutouyrie, P. Segers, A. Donald, and P. Chowienczyk, "Artery society guidelines for validation of non-invasive haemodynamic measurement devices: Part 1, arterial pulse wave velocity," *Artery Res.* **4**(2), 34–40 (2010).
27. H. Obeid, H. Khettab, L. Marais, M. Hallab, S. Laurent, and P. Boutouyrie, "Evaluation of arterial stiffness by finger-toe pulse wave velocity: optimization of signal processing and clinical validation," *J. Hypertens.* **35**(8), 1618–1625 (2017).
28. Y. Chiu, P. Arand, S. Shroff, T. Feldman, and J. Carroll, "Determination of pulse wave velocities with computerized algorithms," *Am. Heart J.* **121**(5), 1460–1470 (1991).
29. E. Hermeling, K. Reesink, R. Reneman, and A. Hoeks, "Confluence of incident and reflected waves interferes with systolic foot detection of the carotid artery distension waveform," *J. Hypertens.* **26**(12), 2374–2380 (2008).